Chinese Chemical Letters 35 (2024) 109756

Contents lists available at ScienceDirect

Chinese Chemical Letters

journal homepage: www.elsevier.com/locate/cclet

A stable Zn-MOF with anthracene-based linker for Cr(VI) photocatalytic reduction under sunlight irradiation

Yan-Kai Zhang[a,b,1], Yong-Zheng Zhang[a,b,1], Chun-Xiao Jia[a], Fang Wang[a], Xiuling Zhang[a,b,*], Yuhang Wu[a], Zhongmin Liu[a], Hui Hu[a], Da-Shuai Zhang[a,b], Longlong Geng[a,b], Jing Xu[a,*], Hongliang Huang[c,*]

[a] Shandong Provincial Key Laboratory of Monocrystalline Silicon Semiconductor Materials and Technology, College of Chemistry and Chemical Engineering, Dezhou University, Dezhou 253023, China
[b] School of Chemistry and Chemical Engineering, Shandong University of Technology, Zibo 255000, China
[c] State Key Laboratory of Separation Membranes and Membrane Processes, School of Chemical Engineering and Technology, Tiangong University, Tianjin 300387, China

ARTICLE INFO

Article history:
Received 16 November 2023
Revised 16 February 2024
Accepted 5 March 2024
Available online 8 March 2024

Keywords:
Metal-organic frameworks
Anthracene-based ligand
Cr(VI) reduction
Photocatalysis
Stability

ABSTRACT

The highly desired goal is to employ visible light for the photocatalytic reduction of toxic Cr(VI) to environmentally friendly Cr(III). Metal-organic frameworks (MOFs) are considered one of the most promising materials for the photoreduction of Cr(VI). Nevertheless, developing MOFs with high stability and activity is still challenging. Herein, we report a stable Zn-based MOF (named **DZU-64**) with an anthracene functionalized ligand, and its reduction of Cr(VI) under sunlight irradiation was investigated. **DZU-64** exhibits excellent chemical stability in pH range of 2−14 aqueous solution, and remarkable thermal stability to 570 °C. For the photoreduction of Cr(VI) under visible light irradiation, **DZU-64** gives a record rate constant of 0.467 min^{-1} and a high Cr(VI) reduction rate of 6.68 mg $Cr_{(VI)}$ $g^{-1}{}_{cata}$ min^{-1} at pH 2. Moreover, under real solar light, **DZU-64** can also efficiently reduce Cr(VI) to Cr(III) while retaining its catalytic activity throughout 5 cycles without any notable decline, further demonstrating its great application prospect. By combining the photovoltaic performance tests and electron spin resonance test, the possible photoreduction of Cr(VI) mechanism in **DZU-64** was analyzed.

Hexavalent chromium (Cr(VI)) finds extensive application across various industrial processes, such as paint-making, leather tanning, and electroplating [1–3]. Due to the good solubility and high toxicity, Cr(VI) wastes are easily released into natural water, posing significant risks to human and environmental health [4,5]. Accordingly, it is crucial to properly dispose of Cr(VI) from the wastewater. Currently, various techniques for eliminating Cr(VI) from waste water have been developed, such as chemical precipitation [6–8], membrane separation [9,10], adsorption [11,12], and reduction [13–15]. Among these techniques, the photocatalytic transformation of Cr(VI) to Cr(III) stands out and ranks among the most promising methods. This is due to its energy efficiency, environmental friendliness, and the ease with which the Cr(III) with low toxicity can be recovered [16–18]. Nevertheless, the majority of photocatalysts, involving ZnO- and TiO_2-based catalysts, and so forth, demonstrate limited reduction performance because of the narrow light absorption, low stability, and low efficiency [19–21]. Thus, the development of new photocatalysts with robust structure and high efficiency for Cr(VI) has become a preferred research focus.

Metal-organic frameworks (MOFs) are advanced crystalline porous materials built from the self-assembly of organic ligand and metal ions [22–24]. Since they combine the advantages of molecular homogeneous and heterogeneous catalysts, MOFs with photoredox activity are of attractive for sustainable photocatalysis and have been extensively study [25–27]. The outstanding porosity and wealth of reactive sites in porous MOF photocatalysts establish the ideal conditions for achieving remarkable catalytic efficiency in their realm [28,29]. Additionally, the capability to design and modify organic ligands at the molecular level offers a convenient avenue for precisely controlling their photoelectric properties [30–34]. It has been found that the utilization of ligands containing photosensitive units or large π-structures can efficiently enhance the photoresponse properties and charge transport efficiency

* Corresponding authors.
E-mail addresses: xlzhang99@126.com (X. Zhang), xujing2306@163.com (J. Xu), huanghongliang@tiangong.edu.cn (H. Huang).
[1] These authors contributed equally to this work.

https://doi.org/10.1016/j.cclet.2024.109756
1001-8417/

of MOFs, and this approach is considered a straightforward and efficient strategy for the development of MOF photocatalysts [35–38]. Due to its excellent optical properties, anthracene, a highly conjugated fused ring, has been widely utilized. By incorporating anthracene groups into the framework, MOFs demonstrate exceptional properties in various applications, including photocatalysis [39–41]. For example, Liu *et al*. synthesized two examples of anthracene-based MOFs that can efficiently degrade tetracycline and RhB in water [42]. Chen *et al*. synthesized a novel anthracene-based Zr-MOF for efficient visible-light-driven CO_2 reduction to formic acid [43]. However, the MOF photocatalysts based on anthracene groups are rare, especially those with robust skeleton to meet the harsh water environment conditions. Therefore, design and synthesis of robust anthracene-based MOFs for efficient reduction of Cr(VI) under visible light even real sunlight exposure is highly desired.

In this work, an anthracene-based MOF (**DZU-64**, DZU = Dezhou University) was synthesized using the 9,10-di(1*H*-pyrazol-4-yl)anthracene ligand (H_2EDP) and Zn^{2+} ions. Single-crystal structure analysis reveals **DZU-64** has a three-dimensional (3D) framework built from the EDP^{2-} linker connecting the 1D Zn-chain. Stability tests show that **DZU-64** has good chemical stability in the pH 2−14 aqueous solutions, and remarkable thermal stability of up to 570 °C. The reduction of Cr(VI) in visible light tests and at room temperature (RT) give the highest rate constant (k) of 0.467 min^{-1} among pristine MOF photocatalysts, to the best of our knowledge. Moreover, in the real atmosphere, **DZU-64** can still effectively convert Cr(VI) to Cr(III) under the irradiation of solar light. Furthermore, a variety of factors influencing the photoreduction of Cr(VI), including the incorporation of a hole scavenger, the acidity of the reaction solution, and the reusability of the catalyst, was also investigated. The possible reduction mechanism of the MOF was analyzed in conjunction with structural analysis, electron spin resonance (ESR), and photovoltaic performance tests.

The H_2EDP ligand is purchased from Jilin Chinese Academy of Sciences-Yanshen Technology Co., Ltd. The brand of *N*,*N*-dimethylformamide (DMF, 99.9%) and acetic acid (HAc, 99.8%) is Sinopharm Chemical Reagent Co., Ltd. and Aladdin Biochemical Technology Co., Ltd. respectively. The remaining commonly used reagents are purchased online and are of analytical grade or higher, ready for direct use. The Bruker D8 ADVANCE X-ray diffractometer was utilized to gather Powder X-ray diffraction (PXRD) patterns, employing Cu-Kα radiation ($\lambda = 0.1542$ nm) within the 2θ range of 5°−50°, while operating the X-ray tube at 40 kV and 40 mA at room temperature. The Shimadzu FTIR-8400S spectrometer was utilized to measure FT-IR spectra. The NETZSCH STA449 F5 thermal analyzer was utilized to perform Thermogravimetry analyses (TGA) in a nitrogen environment. The temperature was increased from ambient temperature to 800 °C at a rate of 10 °C per minute. The Hitachi F4600 luminescence spectrophotometer was utilized to measure the luminescence spectra. The Edinburgh FLS980 fluorescence spectrophotometer was utilized to measure time-resolved PL spectra at room temperature. A Bruker A300 spectrometer was used to obtain ESR spectra. Using a CHI760E electrochemical workstation from Chenhua Instrument in Shanghai, the photoelectrochemical tests were conducted. Gas adsorption was measured by Corrosive gas adsorption analyzer (BSD-PMC). About 120 mg of a clean sample was loaded into a sample tube and evacuated for 6 h at 100 °C in a degassing station to eliminate solvent molecules thoroughly. The crystals were weighed to determine their actual mass and tested for CO_2 adsorption isotherms in a dry ice-acetone bath at 195 K.

In a 20 mL glass vial, H_2EDP (0.1 mmol, 31.04 mg) was dissolved in 8 mL of DMF and $Zn(NO_3)_2{\cdot}6H_2O$ (0.1 mmol, 29.75 mg) was dissolved in 8 mL of deionized water, respectively, then both of them were mixed thoroughly and 240 µL of HAc was added. After ultrasonication for 5 min, it was heated in an oven at 100 °C for 24 h. Yellow rhombic crystals were obtained after cooling to room temperature. After washing by immersion in ethanol for 3 days. The final sample was dried at 100 °C in an oven. Yield: 52% (on the basis of the H_2EDP ligand used). Anal. calcd. (%) for the activated sample (see below) $C_{20}H_{12}N_4Zn$ (%): C, 64.28; H, 3.21; N, 15.00.

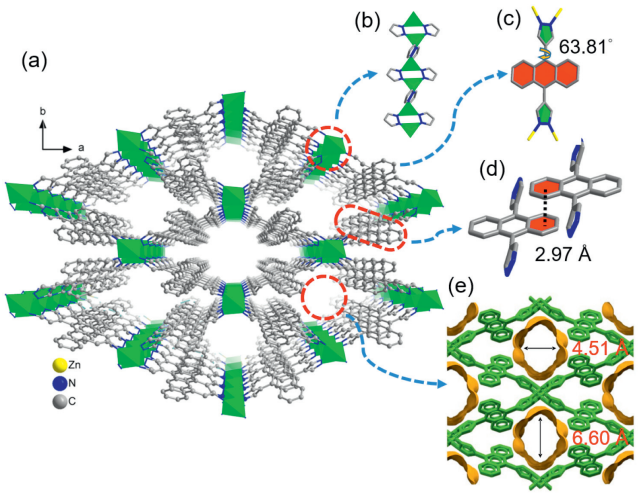

Fig. 1. Schematic of the 3D structure of **DZU-64**, (a) and 1D rod-like building blocks of $Zn(pz)_2$ (b). (c) The dihedral angles between the central anthracene ring and peripheral pyrazolate ring. (d) $\pi\cdots\pi$ distance of the anthracene ring between adjacent ligands. (e) Dimensional schematic of **DZU-64** along *c*-axis 1D channel.

First, 20 mL of 50 ppm $Cr_2O_7^{2-}$ aqueous solution was prepared, and 10 mg of photocatalyst was added to mix evenly. The reaction solution was put into a 30 mL quartz reactor for photocatalytic reduction. The pH of this solution was adjusted using 1 mol/L H_2SO_4 or NaOH. After stirring in darkness for 1 h to achieve adsorption-desorption equilibrium, the reactor was subjected to visible light irradiation (300 W xenon lamp). 1 mL of solution was drawn from the reactor at 5 min intervals during the irradiation process and the diphenylcarbazide (DPC) mentioned was used to analyze the contentions of $Cr_2O_7^{2-}$ through UV–vis spectroscopy [44]. The experimental process is listed below: Initially, a mixture composed 0.2 mL of meticulously prepared 0.25% (w/v) DPC acetone solution, 9 mL of a 0.2 mol/L H_2SO_4 solution, and one milliliter of the $Cr_2O_7^{2-}$ solution was cautiously mixed. The mixture was shaken for 30 s and left undisturbed for 10 min to guarantee full attainment of color formation. Then, UV–vis spectroscopy was utilized to analyze the mixture. At the end of the experiment, the catalyst in the reaction solution was separated by centrifugation and then washed with ethanol. Ultimately, the catalyst underwent a thorough drying process overnight at 100 °C for subsequent experimentation.

DZU-64 was determined to crystallize in the monoclinic crystal system with the space group *C2/c*, as revealed by single-crystal X-ray diffraction (SCXRD) analysis. **DZU-64** presents a three-dimensional (3D) architecture comprising Zn-based rod-like building blocks (RBBs) and EDP^{2-} linkers (Fig. 1a). The Zn^{2+} metal center coordinates with the pyrazole (pz) groups from four EDP^{2-} ligands, exhibiting a tetrahedral coordination geometry (Fig. S1a in Supporting information). Through the alternating arrangement of pz and Zn^{2+} metal centers, 1D undulating RBBs with the chemical formula $Zn(pz)_2$ are generated (Fig. 1b), and the adjacent $Zn(pz)_2$ moieties are linked by the EDP^{2-} ligands. The peripheral pyrazolate and central anthracene rings of EDP^{2-} display dihedral angle of 63.81° (Fig. 1c). Adjacent EDP^{2-} ligands pack in parallel mode, in which the $\pi\cdots\pi$ distance between central anthracene rings is 2.97 Å (Fig. 1d). **DZU-64** displays 1D rectangular channels (the

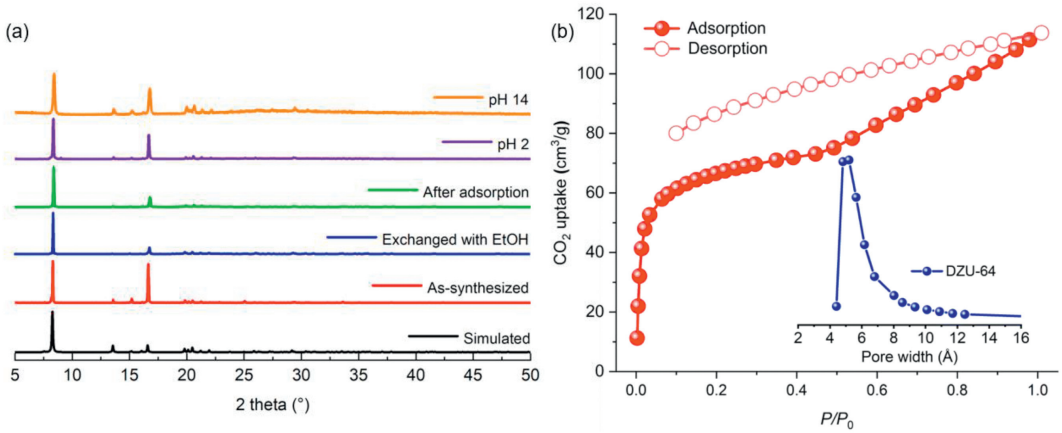

Fig. 2. (a) The synthesized and treated **DZU-64** for PXRD patterns, (b) CO_2 adsorption and desorption isotherms at 195 K of activated **DZU-64**, and the curve of pore size distribution (inset).

distance between the ligands, measured from one wall to another, is 4.51 × 6.60 Å) running along the *c*-axis (Fig. 1e, Figs. S1b and c in Supporting information). It was determined that **DZU-64** had a total solvent-accessible volume of 465.5 $Å^3$, or 24.4% as calculated by PLATON.

Fig. 2a illustrates that the experimental PXRD patterns of as-synthesized **DZU-64** align with its simulated patterns derived from the SCXRD data, suggesting that the material is of high purity. CO_2 adsorption measurement at 195 K was conducted to assess the porosity of **DZU-64** (Fig. 2b). Type IV adsorption isotherms reveal CO_2 uptakes of 118 cm^3/g for **DZU-64** at 1 atm. The Brunauer-Emmett-Teller (BET) surface area, determined through CO_2 adsorption isotherm, is 275.6 m^2/g, and the pore size distribution was estimated to be around 5.20 Å (Fig. 2b). Ideally, a MOF should exhibit stability in water, including both basic and acidic aqueous environments, matters for photocatalytic conversion of Cr(VI) in water system. Fig. 2a demonstrates that **DZU-64** displays exceptional chemical stability and maintains its crystallinity upon exposure to harsh chemical environments, including HCl/H_2SO_4 (pH 2) and NaOH (pH 14) aqueous solutions at RT for 24 h, as evidenced by the consistency in their corresponding PXRD patterns. The SEM images show that **DZU-64** exhibits blocky particles with a crystal size of about 10 μm, and after 1 cycle and 5 cycles of testing, the size of the particles decreased, but the morphology of the sample did not undergo significant changes (Fig. S2 in Supporting information). FT-IR spectra of **DZU-64** and H_2EDP were collected in the range of 4000–400 cm^{-1}. Compared with the H_2EDP, the disappearance of the bending vibration of the N–H bond was observed in the frequency range of 3500-3000 cm^{-1} (Fig. S3 in Supporting information) [45], confirming the coordination between metals and ligands. The thermal stability of MOFs is an important factor for its better application in industrial production. Thermogravimetric analysis shows that **DZU-64** has excellent thermal stability and remains stable up to temperatures as high as 570 °C, as depicted in Fig. S4 (Supporting information).

To investigate the optical absorbance of **DZU-64**, the UV–vis diffuse reflectance spectrum (UV-DRS) was analyzed. As depicted in Fig. 3a, **DZU-64** has the broad range absorption band and strong visible-light absorption from 300 nm to 500 nm, indicating the potential in visible-light photocatalysis. On the basis of the Kubelka–Munk equation of $(\alpha h\nu)^2 = A(h\nu - E_g)$, the calculated bandgap value of **DZU-64** is 2.83 eV, suggesting that **DZU-64** could show a response to visible light (Fig. 3b). Mott-Schottky electrochemical measurements were performed to determine alignment of energy levels in **DZU-64** band-gap structures. The Mott-Schottky diagram in Fig. 3c displays a positive slope, indicating that an n-type semiconductor classification is applicable to **DZU-64** [46], and the flat-band potential value was −0.68 eV *vs.* Ag/AgCl. The flat-band potential is generally considered to be approximately equal to the bottom of the conduction band (CB) in most semiconductors. Hence, the CB edge of **DZU-64** was determined to be −0.44 eV *vs.* the normal hydrogen electrode (NHE), and the corresponding valence band (VB) level was calculated to be 2.39eV *vs.* NHE. On the basis of the above analysis, Fig. 3d schematically shows the energy band diagram of **DZU-64**, revealing the potential of **DZU-64** as a catalyst for the photoreduction of Cr(VI). To assess the separation capabilities of the photogenerated carriers, transient photocurrent measurements and electrochemical impedance spectroscopy (EIS) were performed. Fig. S5a (Supporting information) illustrate the observed photocurrent response of the **DZU-64** electrodes during intermittent cycles of visible-light exposure. The results demonstrate that **DZU-64** is capable of generating electron-hole pairs when stimulated by visible light. EIS test results reveal that the charge-transfer resistance (R_{ct}) of **DZU-64** is about 10 kΩ (Fig. S5b in Supporting information). In general, the above characterization and analysis indicated that **DZU-64** possesses the fundamental characteristics required for its utilization as a photocatalyst.

The adsorption capacity of $Cr_2O_7^{2-}$ on **DZU-64** was initially investigated prior to conducting the photocatalytic experiments, as it plays a significant role in the reduction process of the photocatalyst for $Cr_2O_7^{2-}$ anion [44]. As shown in Fig. S6 (Supporting information), after being immersed in the $Cr_2O_7^{2-}$ solution for 30 min under dark conditions, **DZU-64** can reach adsorption equilibrium, resulting in an uptake of 20 mg/g. Subsequently, the photocatalytic reaction was performed to evaluate the photoreduction performance of **DZU-64**, and the test conditions are as follows: $Cr_2O_7^{2-}$ aqueous solution (20 mL, 50 ppm, pH 2), **DZU-64** photocatalyst (10 mg), tartaric acid (TA, 10 mg), and visible light. Before visible light illumination, the mixture was stirred in the dark for 60 min in order to attain the adsorption-desorption equilibrium of $Cr_2O_7^{2-}$. Fig. 4a illustrates that the concentration of $Cr_2O_7^{2-}$ does not significantly decrease within 30 min when **DZU-64** and TA are not present under visible light exposure. However, a 30% decrease in apparent Cr(VI) is observed for TA, and 70% for **DZU-64**. Impressively, the combination of **DZU-64** and TA demonstrates exceptional photocatalytic activity in reducing Cr(VI), and they could degrade practically 100% of Cr(VI) within 15 min under identical conditions. As shown in Fig. S7 (Supporting information), the binding energies of 586.9 and 578.0 eV correspond to Cr $2p_{1/2}$ and Cr $2p_{3/2}$ of Cr^{3+}, in that order, indicating that $Cr_2O_7^{2-}$ was completely converted to Cr^{3+} through photocatalytic reduction reaction. Fig. S8 (Supporting information) illustrates that the

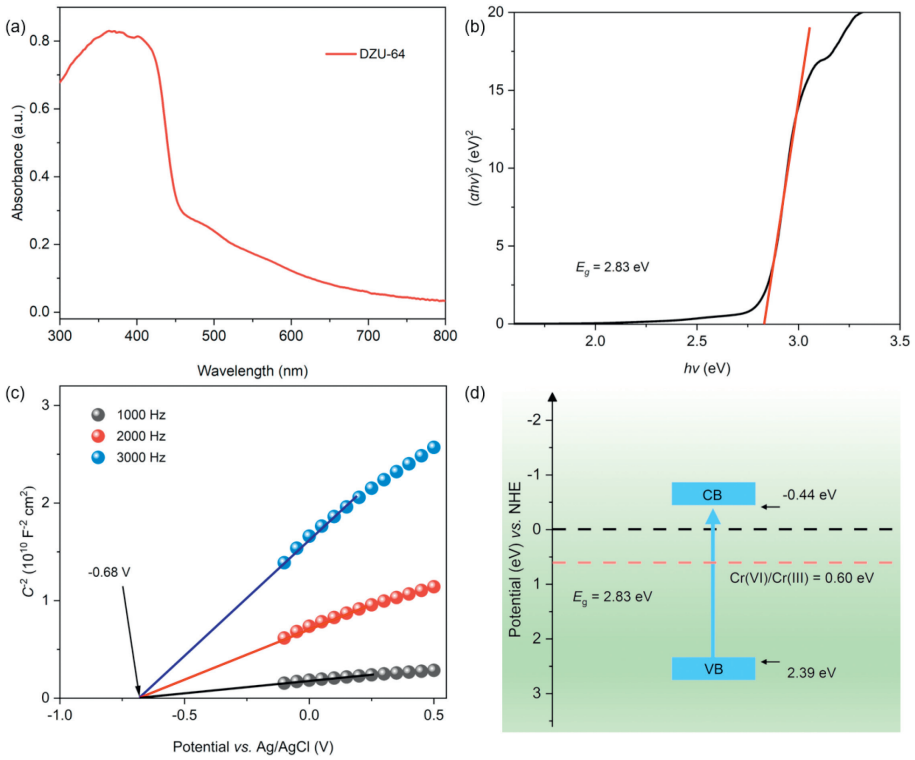

Fig. 3. (a) UV-DRS absorption spectra, (b) band gap, (c) Mott-Schottky plots and (d) schematic of the energy band of **DZU-64**.

photocatalytic reduction of Cr(VI) occurs according to a pseudo-first-order kinetics, under the optimal conditions, and the *k*-value was calculated to be 0.467 min^{-1}. To the best of our knowledge, this is the best catalyst among all the reported pristine MOF photocatalytic material including typical MIL-100(Fe) ($k = 0.013$ min^{-1}), PCN-222 ($k = 0.1289$ min^{-1}), and UiO-66-X (X = NH_2, OH, NO_2, $k = 0.0017–0.0226$ min^{-1}) for the photoreduction of Cr(VI) under simulated visible light irradiation [20,47,48]. Furthermore, the photocatalytic reduction rate of **DZU-64** can reach 6.68 $mg_{Cr(VI)}$ $g^{-1}{}_{cata}$ min^{-1} at the C_0 of 50 ppm, demonstrating a high level of reduction efficiency for Cr(VI) compared to the reported MOF-based photocatalysts (Table S3 in Supporting information).

The presence of hole scavengers is widely recognized to have a significant impact on the rate of photocatalytic process. The main reason for this is the increased efficiency in separating the photogenerated holes (h^+) and electrons (e^-), which happens when the h^+ are quickly depleted. The overall redox reaction, which includes the photoreduction half reaction of Cr(VI), is accelerated as a result. Various electron donors, such as small organic acids and small alcohol, have been utilized to maximize photocatalytic performance by effectively scavenging holes in the photocatalytic reduction of Cr(VI) [49,50]. Herein, TA, oxalic acid (OA), and citric acid (CA) were chosen as a sacrificial agent in order to facilitate the total redox reaction, and the influence of them on the Cr(VI) photocatalytic reduction was demonstrated in Fig. 4b. It is evident that TA significantly enhances the transition of Cr(VI) comparison with other sacrificial agents. Thus, in this Cr(VI) photoreduction system, TA was chosen as the sacrificial agent, and the optimal addition amount is 10 mg TA *vs.* 10 mg **DZU-64**. Besides, to further explore the effects of various free radicals on the reduction process, we used 0.5 mmol/L $AgNO_3$ and 0.5 mmol/L isopropanol (IPA), as a scavenger to capture e^- and $^{\bullet}OH$. Furthermore, the use of N_2 was to remove O_2 in the solution in order to assess the impact of $^{\bullet}O_2^-$ [28]. From Fig. 4c, it can be seen that the addition of $AgNO_3$, IPA, and N_2 inhibited the reduction of Cr(VI) by 43.4%, 78%, and 1.6% respectively within 15 min. The implication is that e^-, $^{\bullet}OH$ and $^{\bullet}O_2^-$ were involved in the reduction of Cr(VI), with e^- making the most substantial contribution.

The pondus hydrogenii of the solution is another crucial parameter for influencing the photocatalytic reduction performance of Cr(VI). Former studies have shown that the photocatalytic reduction activity of Cr(VI) can be enhanced under low pH conditions [51]. Sure enough, the photocatalytic activity of **DZU-64** was observed to exhibit a strong correlation with the pH level (Fig. 4d). At pH 2, **DZU-64** has the capability to fully reduce Cr(VI) when exposed to visible light for a duration of 15 min. However, under identical conditions, the apparent percentage of Cr(VI) reduction significantly decreased to 85%–27% at pH 3–6. Under low acidic conditions, the decrease in photocatalytic activity can be attributed to two factors. Firstly, it is linked to the reduction in the oxidation potential of MOFs, which hinders the catalytic reaction and leads to a decline in photocatalytic activity. Additionally, the formation of $Cr(OH)_3$ precipitate plays a significant role in this decline as well. The formation of this precipitate may obstruct the internal cavities of the framework, effectively covering up the photoactive sites [52]. As a result, the overall photocatalytic activity is further diminished. Consequently, the most favorable pH was 2, and the subsequent research was carried out at this particular pH level.

Furthermore, we verified the photocatalytic reduction performance of H_2EDP ligand and anthracene molecule for Cr(VI) under optimal conditions. As shown in Fig. S9 (Supporting information), the photocatalytic reduction rates of H_2EDP ligand and anthracene molecule were 38% and 45% within 20 min, showing no significant difference but notably lower than that of **DZU-64**. These results indicate that incorporating anthracene groups into the framework of MOF materials is an effective strategy for improving the photocatalytic properties of MOFs.

Inspired by the above excellent results, the photoreduction tests of Cr(VI) of **DZU-64** were performed under real solar light. All other experimental conditions remained unchanged from the sim-

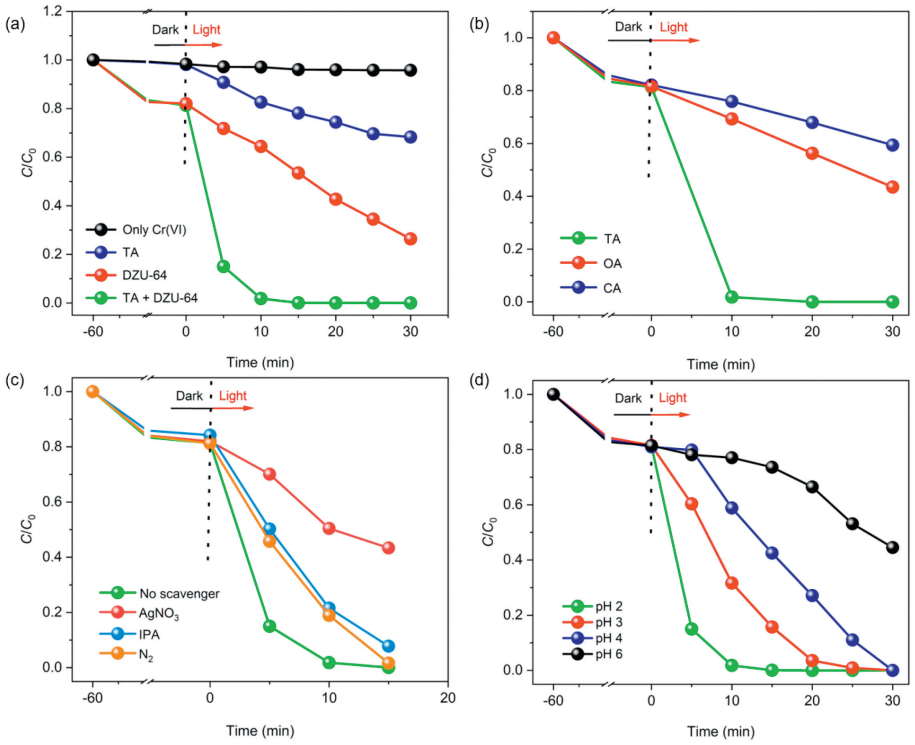

Fig. 4. (a) Photoreduction experiments of Cr(VI) under different conditions. (b) The photoreduction of Cr(VI) with different small organic acids. (c) Effect of addition of trapping agent. (d) The photoreduction of Cr(VI) at varying pH levels.

ulated sunlight irradiation experiments, except for the source of irradiation. The experiment utilizing sunlight was conducted during a sunny period from 9 am to 12 am in May 2023 at the location of Dezhou University (39°44′ N latitude and 116°17′ E longitude, Fig. 5a and Fig. S10 in Supporting information). As depicted in Fig. 5b, the results of the experiment under direct sunlight show that nearly 100% Cr(VI) was reduced to Cr(III) within 35 min when **DZU-64** and TA were added simultaneously. However, only 26% Cr(VI) was degraded without **DZU-64** at the same time, indicating that **DZU-64** could achieve high photocatalytic activity under real sunlight.

The usefulness of a heterogeneous catalyst is largely determined by its capacity to be regenerated and recycled. **DZU-64** was recovered by centrifugation, washed with an ethanol solution, then soaked in ethanol and washed three times with fresh ethanol solution, and finally dried in a vacuum drying oven at 80 °C. The collected sample was used in the next catalytic experiment. The recycling tests conducted under xenon lamp and sunlight irradiation demonstrate that **DZU-64** exhibits excellent stability over 5 cycles of experiments (Fig. 5c and Fig. S11 in Supporting information), and the PXRD spectra of **DZU-64** were tested after 5 cycles of experiments under different light conditions, showing good correspondence of characteristic peaks before and after the experiments, further demonstrating the excellent regenerative performance of **DZU-64** (Fig. S12a in Supporting information). In addition, the CO_2 adsorption isotherms showed that the CO_2 adsorption capacity of **DZU-64** did not decrease significantly before and after the photocatalytic reduction of Cr(VI), confirming that the framework did not collapse or become blocked (Fig. S12b in Supporting information).

ESR spectra measurements were conducted using the **DZU-64** to investigate the generation of e^-. In this study, the capture agent 2,2,6,6-tetramethylpiperidinooxy (TEMPO) was employed. Fig. 6a demonstrates that the TEMPO-e^- signal exhibited a gradual decline with extended illumination and ceased entirely after 2 min, indicating the generation of e^- active species during the photocatalytic reduction process. Meanwhile, $AgNO_3$ was utilized to capture e^- during the Cr(VI) photoreduction process. As illustrated in Fig. 4c, a 43.4% reduction in Cr(VI) was observed within 15 min after the addition of $AgNO_3$, further confirming the e^- participated in the Cr (VI) reduction process. Moreover, as shown in Fig. 6b, the **DZU-64**/TA system display the highest photocurrent density compared to the other two scavengers systems, implying that the most efficient separation and transfer of h^+ and e^- was accomplished in the **DZU-64**/TA system. Besides, the PL spectra of the H_2EDP ligand and **DZU-64** reveal the peaks at 470 nm upon excitation at 300 nm, which indicates there is no ligand-to-metal charge-transfer in **DZU-64** (Fig. S13 in Supporting information).

A plausible mechanism for the photoreduction of Cr(VI) was proposed based on the above experimental results. When **DZU-64** is exposed to irradiation, visible light is absorbed by the photosensitive anthracene nucleus in **DZU-64**, resulting in the production of e^- and h^+. The TA salvager was able to capture h^+ and oxidize it, resulting in the production of H_2O and CO_2 [53], thus hastening the separation of h^+ and e^-, and the generated e^- were accepted by the $Cr_2O_7^{2-}$ ions adsorbed on the pore surfaces of **DZU-64**. Generally, the redox process can be described in the following manner:

$$\text{DZU-64} + h\nu \rightarrow \text{DZU-64}\ (h^+ + e^-) \quad (1)$$

$$Cr_2O_7^{2-} + 14\ H^+ + 6\ e^- \rightarrow 2\ Cr^{3+} + 7\ H_2O \quad (2)$$

$$TA + h^+ \rightarrow CO_2 + H_2O + \text{Other} \quad (3)$$

In summary, we synthesized a new stable Zn-MOF (**DZU-64**) using a photosensitive anthracene-based ligand *via* solvothermal reaction. Notably, the **DZU-64**/TA system demonstrated remarkable

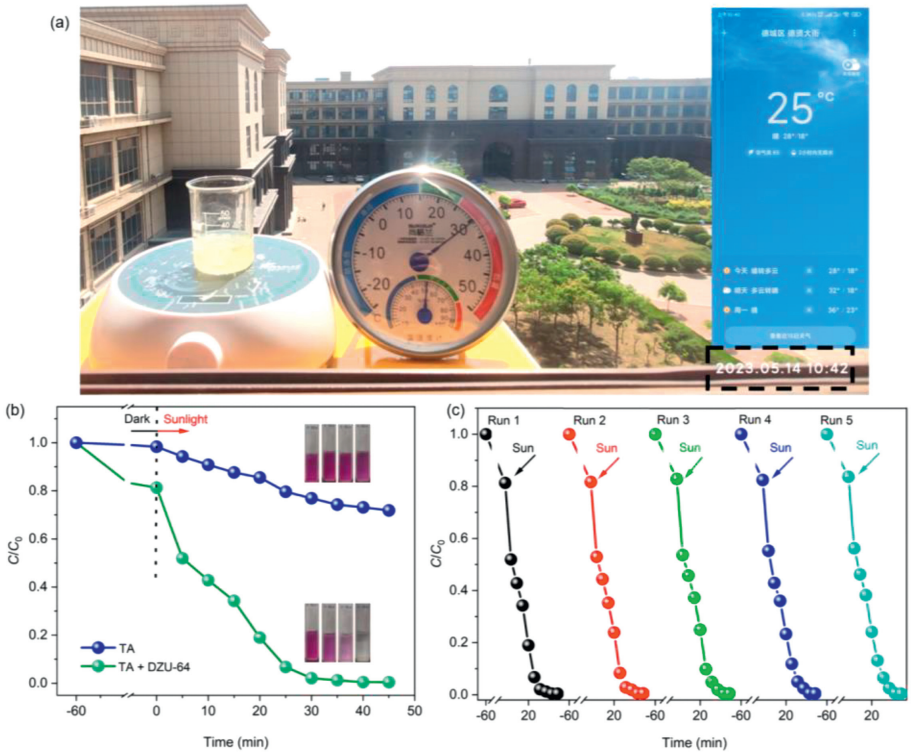

Fig. 5. (a) Photographs of installations that restore Cr(VI) in real sunlight. (b) Cr(VI) photoreduction experiments under sunlight light conditions. (c) **DZU-64** photocatalytic reduction cycling experiment of Cr(VI) under sunlight irradiation.

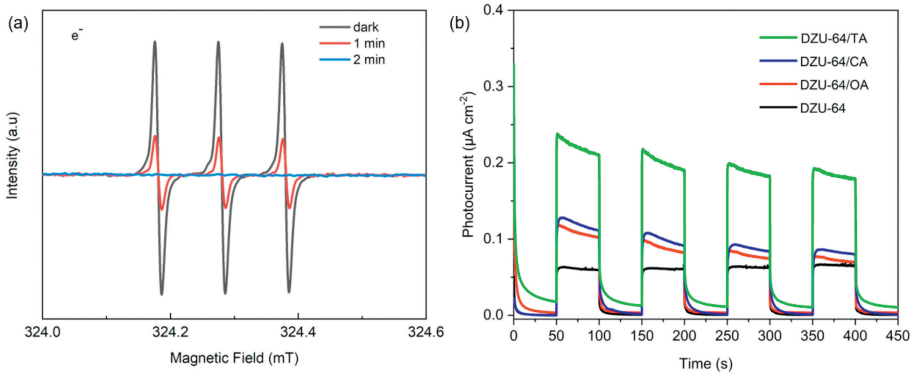

Fig. 6. (a) Electron spin resonance and (b) transient photocurrent measurements in different systems of **DZU-64**.

effectiveness in reducing Cr(VI) in both simulated and real solar light conditions. Additionally, the ESR determinations and quenching tests could further verify the Cr(VI) reduction mechanism in **DZU-64**/TA system. The excellent stability of the **DZU-64** MOF, as well as the exceptional photocatalytic performance of the **DZU-64**/TA system, implies that **DZU-64** has the potential to greatly facilitate Cr(VI) detoxification in practical scenarios.

Declaration of competing interest

The authors declare that they have no known competing financial interests or personal relationships that could have appeared to influence the work reported in this paper.

Acknowledgments

This work was supported by the National Natural Science Foundation of China (Nos. 21601028 and 21902022), the Natural Science Foundation of Shandong Province (Nos. ZR2022QB058, ZR2018LB018 and ZR2019QB026) and Qingchuang Science and Technology Plan of Shandong Province (No. 2021KJ054), the Scientific Research Foundation of Dezhou University (Nos. HXKT2022309, HXKT2022344 and HXKT2022182).

We also would like to thank Shiyanjia Lab (www.shiyanjia.com) for providing the SCXRD data collection, and Jinan Jingshui Biotechnology Co., Ltd. for providing some analysis and testing.

Supplementary materials

Supplementary material associated with this article can be found, in the online version, at doi:10.1016/j.cclet.2024.109756.

References

[1] S. Kamila, P. Shaw, S. Islam, A. Chattopadhyay, Sci. Total Environ. 890 (2023) 164395.
[2] V. Kumar, S.K. Dwivedi, J. Clean. Prod. 295 (2021) 126229.
[3] A. VonHandorf, H.A. Zablon, A. Puga, Semin. Cancer Biol. 76 (2021) 54–60.
[4] J. Liu, S. Sun, H. Zhang, et al., Environ. Res. 237 (2023) 116918.

[5] N.N. Ramli, S.B. Kurniawan, J.O. Ighalo, et al., Biometals 36 (2023) 1189–1219.
[6] W. Li, C. Zhang, X. Wei, et al., Process Saf. Environ. Prot. 165 (2022) 475–486.
[7] J.M. Sun, C. Shang, J.C. Huang, Environ. Sci. Technol. 37 (2003) 4281–4287.
[8] C. Wang, H. Liu, G. Wang, et al., Chem. Eng. J. 450 (2022) 138167.
[9] A. Han, H. Zhang, J. Sun, G.K. Chuah, S. Jaenicke, J. Water Process. Eng. 17 (2017) 63–69.
[10] G. Pugazhenthi, S. Sachan, N. Kishore, A. Kumar, J. Membr. Sci. 254 (2005) 229–239.
[11] D. Pradhan, L.B. Sukla, B.B. Mishra, N. Devi, J. Clean. Prod. 209 (2019) 617–629.
[12] Y. Zhang, J. Wen, Y. Zhou, J. Wang, W. Cheng, J. Hazard. Mater. 458 (2023) 132017.
[13] Z. Guo, M. Cheng, W. Ren, Z. Wang, M. Zhang, J. Hazard. Mater. 430 (2022) 128416.
[14] W.Q. Li, Y.X. Wang, Y.M. Li, et al., J. Clean. Prod. 318 (2021) 128513.
[15] X. Sun, Y. Fang, J. Mu, et al., J. Alloys Compd. 955 (2023) 169969.
[16] Q. Li, Z.Q. Wu, D. Li, et al., J. Mater. Chem. A 11 (2023) 2957–2968.
[17] C.H. Shen, Y. Chen, X.J. Xu, et al., J. Hazard. Mater. 416 (2021) 126217.
[18] Q. Zhuang, H. Chen, C. Zhang, et al., J. Hazard. Mater. 434 (2022) 128938.
[19] M.E. Mahmoud, S.M. Elsayed, S.E.M.E. Mahmoud, R.O. Aljedaani, M.A. Salam, J. Mol. Liq. 347 (2022) 118274.
[20] N. Sharma, A.K. Dey, R.Y. Sathe, et al., Catal. Sci. Technol. 10 (2020) 7724–7733.
[21] H.Q. Zheng, X.H. He, Y.N. Zeng, et al., J. Mater. Chem. A 8 (2020) 17219–17228.
[22] K. Wang, Y. Li, L.H. Xie, X. Li, J.R. Li, Chem. Soc. Rev. 51 (2022) 6417–6441.
[23] Y. Wu, Y. Xie, X. Liu, et al., Coord. Chem. Rev. 483 (2023) 215097.
[24] W. Xu, W. Xue, H. Huang, et al., Catal. B: Environ. 291 (2021) 120129.
[25] Y. Shi, A.F. Yang, C.S. Cao, B. Zhao, Coord. Chem. Rev. 390 (2019) 50–75.
[26] X. Wang, L. Zhu, Z. Lv, et al., Chem. Eng. J. 442 (2022) 136186.
[27] X. Yuan, Q. Mu, S. Xue, et al., J. Energy Chem. 60 (2021) 202–208.
[28] X.H. Yi, Y. Gao, C.C. Wang, et al., Chin. Chem. Lett. 34 (2023) 108029.
[29] C.C. Wang, X. Ren, P. Wang, C. Chang, Chemosphere 303 (2022) 134949.
[30] Y. Chang, H. Huang, T. Yang, et al., J. Colloid Interface Sci. 599 (2021) 785–794.
[31] S. Kampouri, K.C. Stylianou, ACS Catal. 9 (2019) 4247–4270.
[32] Y. Pan, J. Wang, S. Chen, et al., Chem. Sci. 13 (2022) 6696–6703.
[33] K. Wu, X.Y. Liu, P.W. Cheng, et al., J. Am. Chem. Soc. 145 (2023) 18931–18938.
[34] Q. Zhao, X.H. Yi, C.C. Wang, P. Wang, W. Zheng, Chem. Eng. J. 429 (2022) 132497.
[35] X. Feng, Y. Pi, Y. Song, et al., ACS Catal. 11 (2021) 1024–1032.
[36] L. Jiao, J. Wang, H.L. Jiang, Acc. Mater. Res. 2 (2021) 327–339.
[37] Z. Qian, R. Zhang, Y. Xiao, et al., Adv. Energy Mater. 13 (2023) 2300086.
[38] Z. Xin, X. Dong, Y.R. Wang, et al., Adv. Sci. 10 (2023) 2301261.
[39] W. Kong, D. Zhu, Y. Zhang, et al., Angew. Chem. Int. Ed. 62 (2023) e202308514.
[40] J.Y. Zeng, X.S. Wang, Y.D. Qi, et al., Angew. Chem. Int. Ed. 58 (2019) 5692–5696.
[41] Y. Zhao, Z. Shao, Y. Cui, et al., Small 19 (2023) 2300398.
[42] X. Liu, B. Liu, G. Li, Y. Liu, J. Mater. Chem. A 6 (2018) 17177–17185.
[43] D. Chen, H. Xing, C. Wang, Z. Su, J. Mater. Chem. A 4 (2016) 2657–2662.
[44] X.S. Wang, C.H. Chen, F. Ichihara, et al., Appl. Catal. B: Environ. 253 (2019) 323–330.
[45] J.K. Jin, K. Wu, X.Y. Liu, et al., J. Am. Chem. Soc. 143 (2021) 21340–21349.
[46] J. Zheng, Z. Lei, Appl. Catal. B: Environ. 237 (2018) 1–8.
[47] D.D. Chen, X.H. Yi, C. Zhao, et al., Chemosphere 245 (2020) 125659.
[48] A. Valverde, D. Payno, L. Lezama, et al., Adv. Sust. Syst. 6 (2022) 2200024.
[49] Y.X. Li, Y.C. Han, C.C. Wang, Chem. Eng. J. 405 (2021) 126648.
[50] R. Liang, L. Shen, F. Jing, et al., Appl. Catal. B: Environ. 162 (2015) 245–251.
[51] R. Yuan, C. Yue, J. Qiu, F. Liu, A. Li, Appl. Catal. B: Environ. 251 (2019) 229–239.
[52] Q. Wang, L. Wang, S. Zheng, et al., J. Hazard. Mater. 451 (2023) 131149.
[53] R. Djellabi, M.F. Ghorab, Desalination Water Treat. 55 (2015) 1900–1907.